

# Online Unbalance Detection and Diagnosis on Large Flexible Rotors by SVR and ANN trained by Dynamic Multibody Simulations

Oscar García Peyrano,<sup>1,2</sup> Juan Vignolo,<sup>3</sup> Rodrigo Mayer,<sup>3</sup> and Matías Marticorena<sup>1,3</sup>

<sup>1</sup>Balseiro Institute, Cuyo National University, San Carlos de Bariloche, Argentina

<sup>2</sup>GPSignal, San Carlos de Bariloche, Argentina

<sup>3</sup>Vibrations Laboratory, Vibration Division, National Atomic Energy Commission, San Carlos de Bariloche, Argentina

(Received 12 November 2021; Revised 27 January 2022; Accepted 15 May 2022; Published online 01 June 2022)

**Abstract:** Multiple-stage steam turbine generators, like those found in nuclear power plants, pose special challenges with regards to mechanical unbalance diagnosis. Several factors contribute to a complex vibrational response, which can lead to incorrect assessments if traditional condition monitoring strategies are used without considering the mechanical system as a whole. This, in turn, can lead to prolonged machinery downtime. Several machine learning techniques can be used to integrally correlate mechanical unbalance along the shaft with transducer signals from rotor bearings. Unfortunately, this type of machinery has scarce data regarding faulty behavior. However, a variety of fault conditions can be simulated in order to generate these data using computational models to simulate the dynamic response of individual machines. In the present work, a multibody model of a 640 MW steam turbine flexible rotor is employed to simulate mechanical unbalance in several positions along the shaft. Synchronous components of the resulting vibration signals at each bearing are obtained and utilized as training data for two regression models designed for mechanical unbalance diagnosis. The first approach uses an artificial neural network and the second one utilizes a support vector regression algorithm. In order to test their performance, the stiffness of each bearing in the multibody simulation was altered between 50% and 150% of the training model values, random noise was added to the signal and several dynamic unbalance conditions were simulated. Results show that both approaches can reliably diagnose dynamic rotor unbalance even when there is a typical degree of uncertainty in bearing stiffness values.

**Keywords:** condition monitoring; mechanical unbalance; machine learning; steam turbine

## I. INTRODUCTION

Multistage steam turbine generators are central to a significant portion of baseline power generation worldwide and, thus, are required to operate continuously for extended periods of time [1]. These machines are therefore constantly monitored through various techniques such as performance analysis, oil analysis, and vibration analysis to ensure safe, dependable, and reliable operation and to minimize downtime losses through condition-based maintenance [2].

This paper focuses on online detection and diagnosis of mechanical unbalance in these types of rotors. This is one of the main causes of synchronous vibration in turbomachinery which can shorten the lifespan of bearings, seals, and other machine components if allowed to reach excessive levels. Turbine generators consisting of several coupled high and low pressure stages show flexible rotor behavior, which pose additional challenges with regards to identifying and correcting rotor unbalance [3]. Several factors contribute to a complex rotor dynamic response in these rotors, such as nonhomogeneous bearing stiffness coefficients, multiple potential planes of unbalance, presence of misalignment between rotor shafts and fluid dynamic effects, among others. Under these conditions it becomes harder to isolate the

different sources of vibration from transducer signals using traditional signal processing techniques. Furthermore, even when unbalance is the root cause of an increment in rotor synchronous vibration, some of the above factors can obscure the source of this increment (i.e. the position of the unbalanced plane along the rotor). Thus, in such complex systems, it becomes necessary to integrate information from several physical signals so as to properly correlate them with mechanical faults. However, the available vibration data corresponding to various types of faults on a particular steam turbine generator will likely be limited. Therefore, dynamic modeling of rotor-bearing systems becomes a key tool for understanding how machine vibrations arise from particular faults. Given that these machines have high costs associated with downtime, it is especially important to identify the unbalance state previous to any scheduled maintenance.

Multibody simulation (MBS) uses numerical methods to solve the nonlinear equations of motion with respect to time of machine elements that undergo large displacements. The mechanical system is modeled in the form of individual rigid bodies which can be coupled together with constraint equations. This methodology has been used to model unbalance in coupled dual-rotor systems [4]. By modeling a multistage steam turbine in this way, any number of unbalance conditions can be simulated, and the vibrational response along the shaft can be obtained. Afterwards, a machine learning algorithm can be used to generate a

Corresponding authors: Oscar García Peyrano, Matías Marticorena (e-mails: [garciapeyrano@yahoo.com.ar](mailto:garciapeyrano@yahoo.com.ar); [matias.marticorena@cab.cnea.gov.ar](mailto:matias.marticorena@cab.cnea.gov.ar)).

*meta-model* of the system that can receive vibration signals and output the unbalance state on all stages.

In recent decades, several machine learning approaches have been explored and incorporated into machine fault diagnosis, as they offer the possibility to adaptively learn the diagnosis knowledge of machinery from previously collected data [5–11]. Key features can be extracted from a variety of transducer signals and correlated to different machine health states to perform online diagnosis. This strategy can be used with classification algorithms, for anomaly detection and to identify certain types of faults [8,9], or with regression algorithms, to model and predict dynamic behavior [6,10–12]. Physics-informed machine learning refers to the integration of real world data and mathematical physics models even in partially understood, uncertain contexts [13]. Recently, physics-informed machine learning approaches have been proposed to structural health monitoring [14] and to predict the dynamics of specific machine tools [15] among others.

In the present work, a regression approach is employed to map various states of mechanical unbalance on a multi-body model of a steam turbine onto the rotor's vibrational response on each measuring point, in order to generate a regression model (RM) of the rotor bearing system. Two machine learning methods are trained using MBS data: an artificial neural network (ANN) and a support vector regression (SVR) algorithm. Their diagnosis performance is then evaluated using data from a modified MBS model in order to address the issue of signal noise and parameter uncertainty.

## II. PROPOSED METHOD

Vibration data corresponding to a range of unbalanced conditions were generated using a flexible MBS of a 640 MW steam turbine generator.

The two RMs were designed in such a way that they can receive data extracted from rotor bearing vibrations as inputs and generate a prediction of the magnitude and angle of unbalance at 10 locations along the shaft that gave origin to those vibrations.

Figure 1 illustrates the training process of a generic RM and its use for unbalance diagnosis. The MBS model that generates training data should be properly modified if changes in mechanical parameters take place, followed by a re-training of the RM.

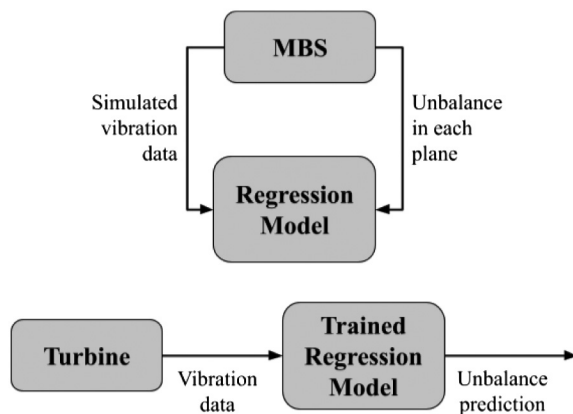


**Fig. 1.** Diagram showing supervised training of a RM with simulated data and its use for rotor unbalance diagnosis.

## A. MULTIBODY SIMULATION OF A STEAM TURBINE GENERATOR ROTOR

A dataset for the RMs was generated via a dynamic MBS model of a 640 MW steam turbine generator. The model is a simplified version of the former steam turbine found in Embalse nuclear power plant in Córdoba Province, Argentina (Fig. 2).

The rotor is 55.7 m long and weighs approximately 350 tons. It has one high pressure stage, three low pressure stages, and a synchronous generator, each one supported by two journal bearings (10 in total). Lateral displacement is measured at each bearing on the horizontal plane. Point masses can be placed at radius of 1000 mm on the balancing planes at the end of each turbine stage and generator in order to simulate unbalance. Figure 3 shows a visual representation of the model. The first rotor corresponds to the high pressure stage, followed by the three low pressure stages and the generator rotor. Of these, the low pressure stages are where the causes of vibration generally arise.

The MBS model consists of several interconnected rigid body elements, in a *lumped parameter* configuration, as shown in Fig. 4.

In order to represent rotor flexibility, each rigid shaft element is connected to the next by a kinematic pair or *joint* which allows rotational movement around the vertical axis and the horizontal axis perpendicular to the shaft centerline. Additionally, these joints have rotational stiffness values assigned to them, which relate to shaft flexural stiffness through the following equation:

$$k_{rot} = \frac{EI}{l} \quad (1)$$

where  $E$  is the elastic modulus of the shaft,  $I$  its moment of inertia, and  $l$  is the length of each segment [16].

The equations of motion of multibody systems can be obtained using Lagrange's equations with an augmented formulation for kinematic constraints and can be written in the following form [17]:

$$[M]q + [C_q]^T \lambda = Q_e + Q_v \quad (2)$$

where  $[M]$  is the mass inertia matrix,  $[C_q]$  the constraint Jacobian matrix,  $\lambda$  the vector of Lagrange multipliers,  $Q_e$  the vector of generalized forces, and  $Q_v$  the vector of quadratic velocity inertia forces.  $Q_e$  can be derived using the principle of virtual work on locally applied forces,  $F^{mn}$



**Fig. 2.** Embalse nuclear power plant turbine generator.

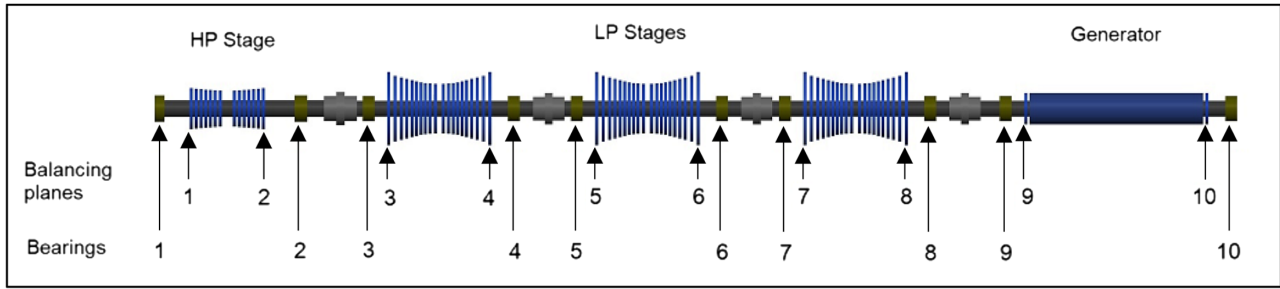


Fig. 3. MBS model of a 640 MW steam turbine generator rotor with 10 bearings and 10 balancing planes.

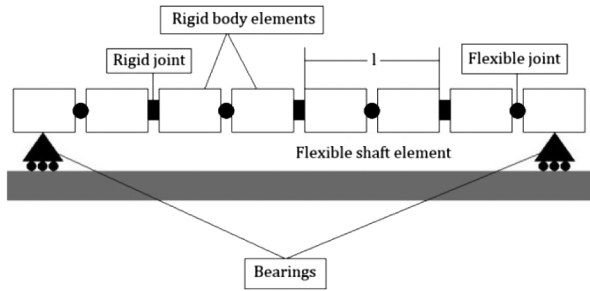


Fig. 4. Lumped parameter configuration of the turbine shaft between two bearings.

and moments  $T^{mn}$ , acting on element  $m$  due to interaction with body  $n$ . These, in turn, can be obtained as follows:

$$\begin{bmatrix} F^{mn} \\ T^{mn} \end{bmatrix} = - \begin{bmatrix} K_b \\ D_b \end{bmatrix} \begin{bmatrix} d^{mn} \\ \dot{\theta}^{mn} \end{bmatrix} \quad (3)$$

where  $d^{mn}$  and  $\theta^{mn}$  are the relative translational and rotational displacements between elements and  $[K_b]$  and  $[D_b]$  are the stiffness and damping matrices. The latter are  $6 \times 6$  symmetrical matrices, which correlate forces with displacements and velocities between bodies in all degrees of freedom. In the model, of three only two rotational degrees of freedom remain unconstrained regarding movement between shaft elements. Thus,  $[K_b]$  and  $[D_b]$  take the form:

$$[K_b] = \begin{bmatrix} k_{11} & \cdots & k_{1N} \\ \vdots & \ddots & \vdots \\ k_{N1} & \cdots & k_{NN} \end{bmatrix} \quad (4)$$

$$[D_b] = \begin{bmatrix} d_{11} & \cdots & d_{1N} \\ \vdots & \ddots & \vdots \\ d_{N1} & \cdots & d_{NN} \end{bmatrix} \quad (5)$$

Stiffness coefficients  $k_{44} = k_{55} = \frac{EJ}{l}$  and  $k_{ij} = 0$  for all other  $i, j$ . Additionally, for body elements linked to one of the journal bearings, bearing stiffness acts on both lateral directions ( $k_{11}$  and  $k_{22}$ ). Only one of such elements,  $k_{33}$ , will have a stiffness coefficient acting on the axial direction to represent the rotor's thrust bearing. In  $[D_b]$ , similarly,  $d_{ij} = 0$  for  $i \neq j$ . Lateral damping coefficients  $d_{11}$  and  $d_{22}$  act on elements linked to journal bearings, and axial coefficient  $d_{33}$  acts on the thrust bearing. Rotational coefficients  $d_{44} = d_{55}$  represent the shaft internal friction. There is a nonzero damping coefficient  $d_{66}$  which represents bearing friction forces produced by shaft rotation.

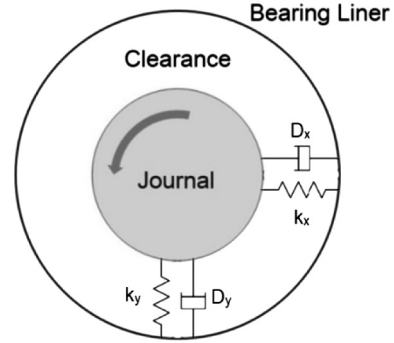


Fig. 5. Linear journal bearing model.

Bearings were modeled as shown in Fig. 5, with two linear springs 90 degrees apart. Viscous damping was modeled in the same way.

**1) FEATURE EXTRACTION.** The MBS outputs one displacement signal for each bearing. For unbalance diagnosis purposes, only the synchronous component of those signals (1X vibration) is relevant. Therefore, for each simulation of an unbalanced state, 10 1X vibration values will be obtained using a Fast Fourier Transform algorithm. These values are complex numbers whose absolute values and arguments represent the 1X vibration magnitude and phase, respectively, at each bearing.

## B. ARTIFICIAL NEURAL NETWORK ALGORITHM

This study employed a sequential ANN, where models are created layer by layer and each one has only one input and one output tensor. Layers are dense, meaning each neuron is connected to every neuron in the following layer and the "Adam" optimization algorithm was used [18]. Since the network output is a floating-point tensor, the root mean square error (RMSE) formula was selected as the algorithm loss function [19]. RMSE was computed according to the following formula:

$$RMSE = \sqrt{\frac{\sum_{i=1}^n (y_i^p - y_i^s)^2}{n}} \quad (6)$$

where  $y_i^p$  is the predicted value for a given sample,  $y_i^s$  is the corresponding simulated value, and  $n$  is the number of samples.

For the neural network (NN) model, a 1-hidden layer model was proposed. In order to obtain the optimal number of neurons in this layer, several NN models were trained

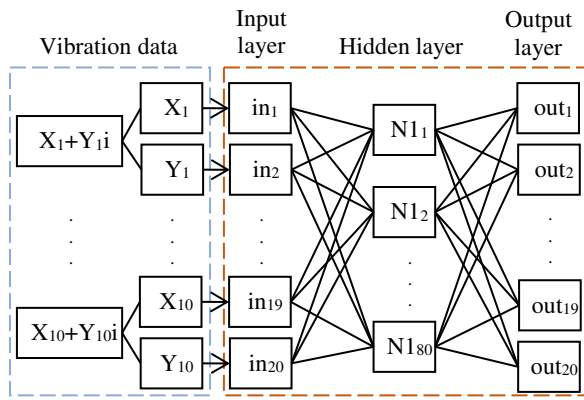


**Fig. 6.** Architecture of the ANN for rotor unbalance diagnosis of a rotor with 10 bearings and 10 balancing planes.

varying this amount and the RMSE metric was calculated for each case. Figure 6 shows the architecture of the ANN.

The first layer has 20 input values corresponding to the real and imaginary parts of the 10 complex values from MBS 1X vibration data. The output layer yields 20 values which are the real and imaginary parts of the predicted unbalance in each balancing plane. These values were expressed as complex numbers for later efficacy evaluation purposes. Their moduli and argument represent unbalance magnitude and angle, respectively.

Another parameter that needs to be defined for the NN model is the number of iterations of the data set. To evaluate this, several networks were trained varying this parameter between 1 and 2000, obtaining the RMSE for each model.

### C. SUPPORT VECTOR REGRESSION

Support vector machine (SVM) algorithms were developed by Vapnik et al [20] based on statistical learning theory. Although SVMs were originally intended to solve binary classification problems, they are currently used to solve various types of problems, including regression problems through the use of SVR. The basic idea of SVR is to map the training data  $x \in X$ , to a higher dimensional space  $F$  through a nonlinear mapping  $\phi: X \rightarrow F$ , where a linear regression can be performed.

Considering the training data:  $\{(x_1, y_1), \dots, (x_n, y_n)\}$ , where  $x_i \in \mathbb{R}^d$  and  $y_i \in \mathbb{R}$ . Let  $\phi: X \rightarrow F$  be the function that makes each input point  $x$  correspond to a point in the feature space  $F$ . The goal is to translate the data points into this new feature space where the function that best approximates the outputs of our set can be found. In a general case, said function will be as follows:

$$f(x) = w \cdot \phi(x) + b \tag{7}$$

The optimization problem (also called primal problem) can be represented by the following equations:

$$\begin{aligned} & \text{minimize} \quad \frac{1}{2} \|w\|^2 + C \sum_{i=1}^n (\xi_i + \xi_i^*) \\ & \text{subject to} \quad y_i - \langle w, \phi(x_i) \rangle \leq \varepsilon + \xi_i \quad i = 1, \dots, n \\ & \quad \langle w, \phi(x_i) \rangle - y_i \leq \varepsilon + \xi_i^* \quad i = 1, \dots, n \\ & \quad \xi_i \geq 0, \quad \xi_i^* \geq 0 \quad i = 1, \dots, n \end{aligned}$$

In this expression,  $\xi_i$  and  $\xi_i^*$  are the Lagrange slack variables, while  $\varepsilon$  represents the error threshold, the value below which the regression algorithm ignores the error at the moment of fitting the training sample.

The parameter  $C$  is always positive and determines the balance between the model complexity and the bias. The larger it is, the more likely the RM is to overfit, while smaller values of  $C$  lead to under-fitting. In SVR models,  $C$  is a hyperparameter which is set by the user.

The Lagrangian dual problem for this case can be represented by the following formulation:

$$\begin{aligned} & \text{maximize} \\ & -\frac{1}{2} \sum_{i,j=1}^n (\alpha_i - \alpha_i^*)(\alpha_j - \alpha_j^*) \langle \phi(x_i), \phi(x_j) \rangle \\ & -\varepsilon \sum_{i=1}^n (\alpha_i + \alpha_i^*) + \sum_{i=1}^n y_i (\alpha_i - \alpha_i^*) \end{aligned}$$

subject to

$$\sum_{i=1}^n y_i (\alpha_i - \alpha_i^*) = 0 \quad \alpha_i, \alpha_i^* \in [0, C]$$

It can be seen that the objective function only depends on  $\langle \phi(x_i), \phi(x_j) \rangle$ . As an alternative to solving this calculation in the space  $F$ , which can be computationally intensive for problems with high dimensionality, the algorithm instead defines a kernel function  $K: X \times X \rightarrow \mathbb{R}$ , which assigns a real value to each pair of elements of the input space  $X$ . The new value refers to the scalar product of the images of said elements in the new space  $F$ , that is,

$$K(x, x') = \langle \Phi(x), \Phi(x') \rangle \tag{8}$$

where  $\Phi: X \rightarrow F$ .

In this study, three SVR kernels were utilized to solve the unbalance mapping problem: the linear kernel, the second-degree polynomial kernel, and the radial basis function (RBF) kernel. These three can be expressed by the following equations, respectively:

$$K(x, x') = \langle x, x' \rangle \tag{9}$$

$$K(x, x') = (\gamma \langle x, x' \rangle)^2 \tag{10}$$

$$K(x, x') = \exp(-\gamma \|x - x'\|^2) \tag{11}$$

In these expressions,  $\gamma$  is a hyperparameter set by the user.

### D. TRAINING PROCEDURE

A data set was generated using the MBS model by simulating a random unbalance value between 100000 *gmm* and 150000 *gmm* placed at a random angle on the balancing planes of the MBS training model. On each individual rotor, the two discs closest to rotor bearings were used as balancing planes. This was achieved by placing a point mass between 100 and 150 grams at a distance of 1000 mm from the shaft centerline.

Two types of unbalance were used: single plane and two plane. For single-plane unbalance, the mass was placed on one balancing plane at a time and this was repeated for each of the 10 planes. For two-plane unbalance, a pair of masses was placed with a 180° angle difference on every

possible combination of two balancing planes. Additionally, residual unbalance was added by placing point masses between 1 and 10 grams on each balancing plane, at random angles.

All these cases add up to a set of 55 training runs. Each set of training runs was simulated 20 times in order to generate additional data with different values of residual and single or two-plane unbalance within the given range, giving a total of 1100 unbalance cases. 80% of these cases were used as training dataset for the RMs. The remaining 20% were used as testing dataset.

**E. EVALUATION AND COMPARISON**

In order to assess the efficacy and robustness of each approach, four unbalance scenarios were simulated. A second multibody model was employed for this purpose, which included variations of bearing stiffness and nonperiodic forces. The stiffness parameters of each bearing in the second MBS model were set between 50% and 150% of the value used for generating training data, with the purpose of representing the uncertainty in stiffness coefficients. Noise was also added to signals in the form of an input radial force on both the horizontal and vertical directions, which took random values between 0 and 250 N on each time step, so as to take into account nonideal operating conditions which affect vibration signals.

The following unbalance conditions were simulated using the second MBS model described above. It should be emphasized that these cases were used to evaluate the proposed method and differ from the dataset employed for training and testing the RMs:

- Case 1: 75000  $gr \cdot mm$  at  $107^\circ$  on balancing plane 5
- Case 2: 75000  $gr \cdot mm$  at  $248^\circ$  on balancing plane 1
- Case 3: 75000  $gr \cdot mm$  at  $252^\circ$  on balancing plane 9 and 75000  $gr \cdot mm$  at  $162^\circ$  on plane 10
- Case 4: 75000  $gr \cdot mm$  at  $164^\circ$  on balancing plane 3 and 75000  $gr \cdot mm$  at  $74^\circ$  on plane 8

The simulated 1X vibrations for each case were used to estimate the unbalance on each balancing plane with both RMs and the accuracy of the estimations was assessed.

As an example to show the rotor behavior, case 1 (unbalance on plane 5) is analyzed. Figure 7 shows the 1X vibration magnitude on each bearing. Figure 8 displays the shaft orbits on the first and fifth bearing.

The fifth bearing, despite being closest to where the unbalance weight was placed, has the second smallest 1X

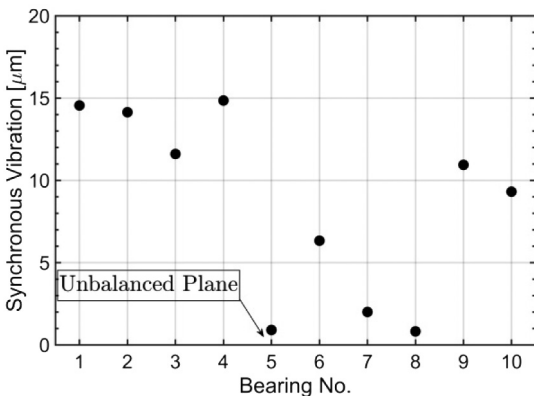


Fig. 7. 1X vibration magnitude on rotor bearings for case 1.

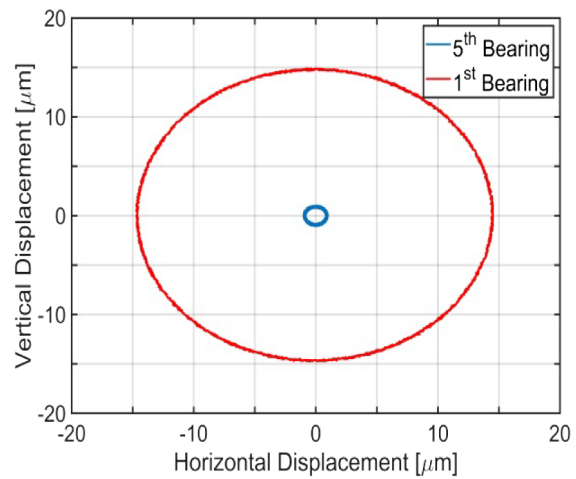


Fig. 8. Rotor orbits on the first and fifth bearing for case 1.

response. Meanwhile at the first and fourth bearings, where only residual unbalance was simulated, amplitudes are almost 15 times higher. This example illustrates that, in complex rotor dynamic systems, vibration amplitude alone is insufficient to determine its root cause.

Relative displacement of the turbine shaft with respect to the fifth and first bearings is shown on Figs. 9, 10,

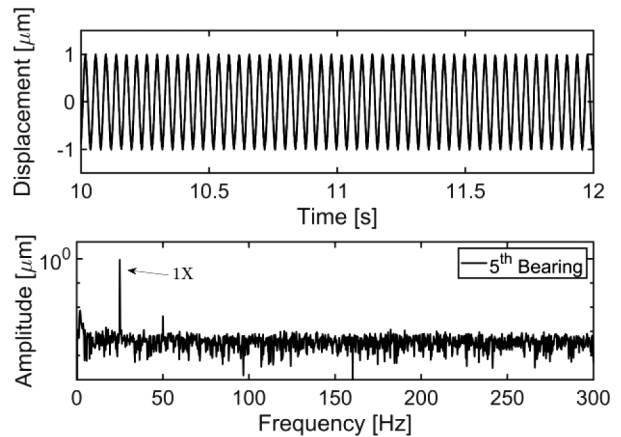


Fig. 9. Relative displacement of the shaft on the fifth bearing, for case 1.

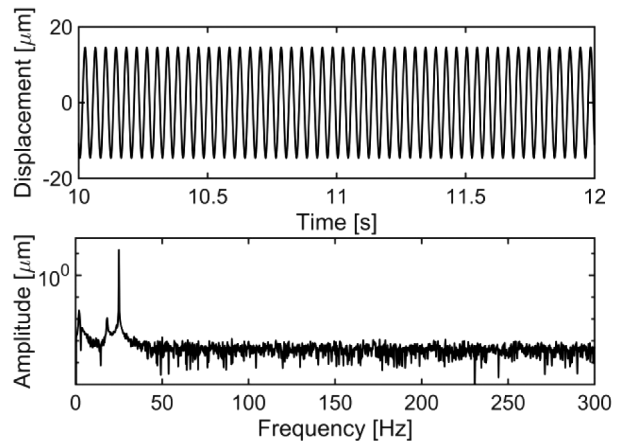


Fig. 10. Relative displacement of the shaft on the first bearing, for case 1.

respectively. Time history signals are portrayed above and their frequency spectra below.

The simulated vibrations have amplitude values in the order of those typically found in large nuclear steam turbines at nominal speed [21]. The time history responses have some noise content in the low frequency range, mainly due to rotor modal response, and in the high frequency range, due to the random radial force included in the simulations. The frequency spectrum of the fifth bearing also shows 2X (50 Hz) harmonic content. Rotor response to unbalance reflects on the 1X amplitude. Its magnitude and angle were obtained by using fast Fourier transform after performing time synchronous averaging of the vibration signal in order to reduce any noise that could be distorting the 1X component.

### III. RESULTS AND DISCUSSION

#### A. ANN PARAMETER ANALYSIS AND OPTIMIZATION

Table I shows the RMSE values obtained from training several ANNs like that shown in Fig. 6 with different amounts of hidden layer neurons.

The NN models show that significantly smaller errors were found for 20 neurons or higher. Because of the lesser associated complexity, a 20-neuron layer was chosen for the ANN to be tested with various data set iterations.

#### B. RMSE vs. NUMBER OF DATA SET ITERATIONS

Figure 11 shows RMSE plotted against number of iterations on the training dataset for the ANN model. It can be seen that the error stabilizes after 500 iterations, therefore this value was chosen for the RM for unbalance diagnosis.

**Table I** RMSE for NNs with different number of neurons on the hidden layer

Neurons in hidden layer	RMSE [gr-mm]
10	26000
15	16403
20	182.5
25	12
30	70

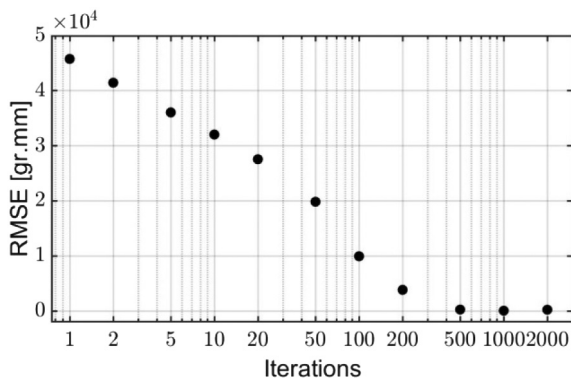


**Fig. 11.** RMSE vs. number of dataset iterations.

#### C. SVR PARAMETER ANALYSIS AND OPTIMIZATION

As mentioned before, for the SVR models, three kernels were proposed: linear, second-degree polynomial, and RBF. The next step was to determine the best parameters for each kernel. In order to accomplish this, an exhaustive search was carried on, optimized by cross-validation. The parameter C could vary between  $10^{-2}$  and  $10^{10}$ , and  $\gamma$ , between  $10^{-9}$  and  $10^3$ . This analysis led to the set of results shown on Table II.

Once the parameters were determined, the data set generated by the training model was split between training and testing data, with an 80% – 20% ratio. Using these, each kernel was trained again, and the results were evaluated by the RMSE metric, as presented in Table III.

It can be seen that the second degree Poly kernel has a poor performance in comparison to the other two cases, a behavior that could be attributed to convergence issues. Due to its higher performance and inherent simplicity, the linear kernel was chosen in order to continue the study.

#### D. PERFORMANCE OF THE RMS FOR DYNAMIC UNBALANCE DIAGNOSIS

In this section, results from both RMs regarding each of the four unbalance scenarios generated by the second MBS model are presented. Figure 12 simulated values of residual and severe unbalance on each balancing plane, alongside those calculated by the ANN and SVR models.

Both magnitude and angle are plotted for each unbalance scenario, but angles are only shown for planes with severe unbalance.

In all four cases, severe unbalance values calculated by the RMs differ from those simulated in the second MBS model by less than 12%. Residual unbalance values have similar error relative to the simulated severe unbalance (75000 gr-mm).

The relative error between simulated and RM-predicted values was calculated as follows:

$$\frac{\Delta U_k}{|U_{ref}|} = \frac{||U_k^p| - |U_k^s||}{|U_{ref}|} \quad (12)$$

where  $\Delta U_k$  is the difference between the predicted and simulated unbalance moduli at the  $k^{th}$  plane. The reference value  $|U_{ref}| = 75000 \text{ gmm}$  is the unbalance being used as severe unbalance on the simulations performed with the second MBS model. Table IV shows the maximum relative

**Table II** Results for SVR kernel parameter analysis

Kernel	$\gamma$	C
Linear	-	1
Second degree Poly	$10^{-9}$	0.01
RBF	$10^{-6}$	1000000.0

**Table III** RMSE of each SVR kernel.

Kernel	RMSE [gr-mm]
Linear	1989
2 <sup>nd</sup> degree Poly	40550
RBF	4509

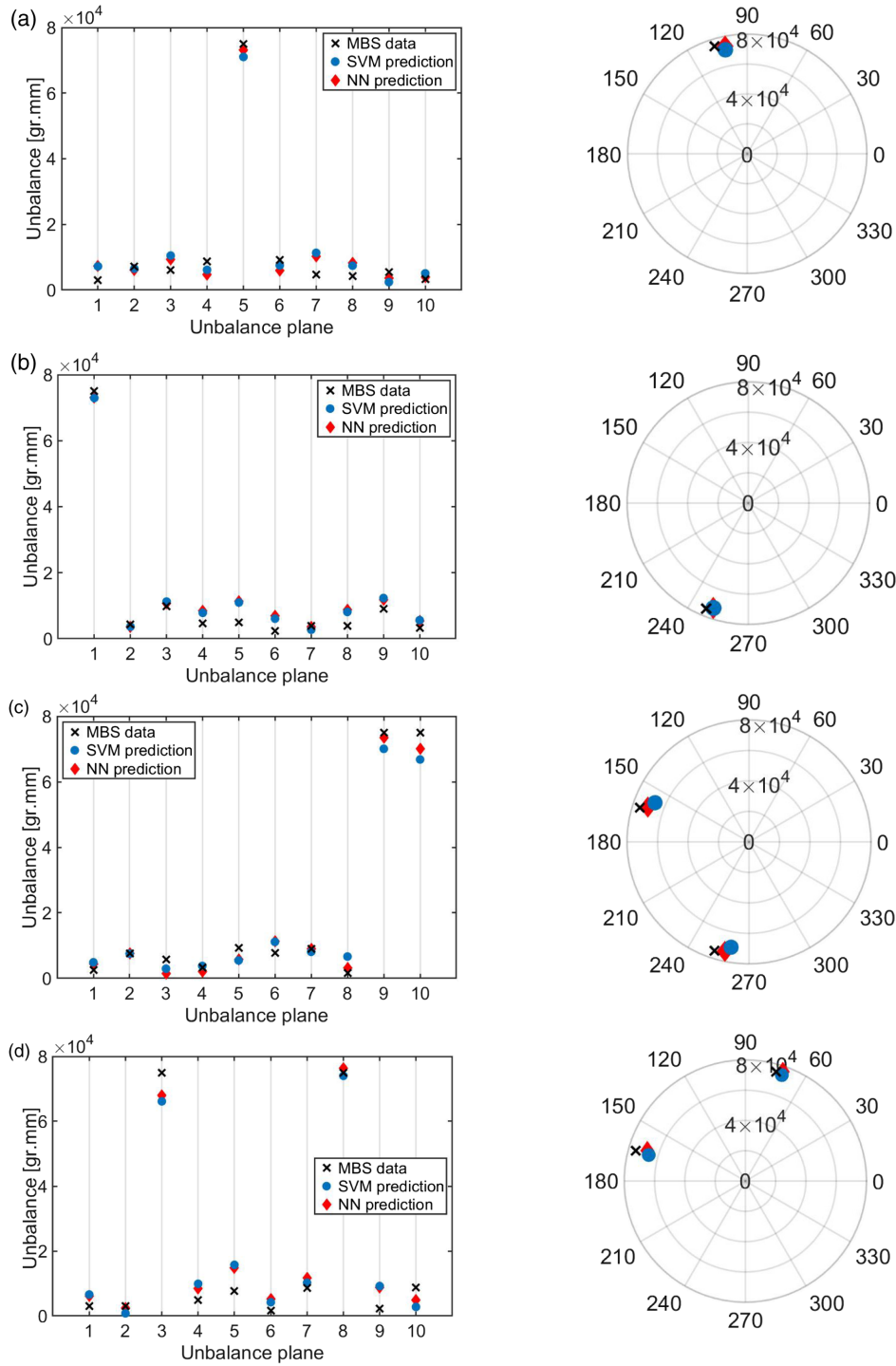


**Fig. 12.** Simulated vs. predicted unbalance. On the left: unbalance magnitude for each plane. On the right: polar plot for planes with severe unbalance. a) Case 1. b) Case 2. c) Case 3. d) Case 4.

**Table IV** Maximum relative errors of SVR and ANN models for each unbalance scenario

	SVR (%)	ANN (%)
Case 1	8.7	7.3
Case 2	8.0	8.6
Case 3	10.9	6.6
Case 4	11.8	9.5

errors of both RMs for each of the four unbalance scenarios simulations. SVR shows somewhat higher errors on two-plane unbalance predictions. Besides this, no significant advantages were found between the results yielded either by the ANN or by the SVR regression models. However, an aspect that should be taken into account when designing condition monitoring strategies is that of complexity and reliability. Although the ANN achieved slightly more accurate predictions, its internal model cannot be inspected, which adds a degree of uncertainty to its application [22].

This method is effective for discriminating between severe and residual unbalance. For the purposes of this work, unbalances below  $10^4$  gr-mm were considered residual. Adequate follow-up of values above this limit through continuous monitoring, in combination with RMs of this kind, can alert operation and maintenance personnel of developing unbalance on its early stages.

The RM calculated angles also approximate simulated ones with enough precision so as to be of value for condition monitoring of unbalance, with differences smaller than  $8^\circ$ . Monitoring of 1X vibration angles can help differentiate between mechanical unbalance and other faults that also cause an increase of 1X vibration amplitude, like magnetic unbalances due to stator field asymmetries and looseness of foundation elements. In such cases, these angles will not remain constant, as with mechanical unbalance.

Linear stiffness and damping coefficients were used on both MBS models, which are adequate for machines of this scale operating at supercritical speeds [21]. For simulations involving resonances or other high amplitude displacements, nonlinear stiffness coefficients should be utilized instead.

#### IV. CONCLUSIONS

The online unbalance diagnosis of a large multistage steam turbine generator was addressed in this paper. The proposed method utilizes a MBS dynamic model of the rotor bearing system to generate vibration data from a series of representative unbalance conditions. A RM is then trained using these data, so that the unbalance condition of the machine being modeled can be rapidly calculated from the synchronous vibration measured at its bearings. The MBS can be periodically revised to follow any relevant changes in the mechanical and operational characteristics of the machine, so that the RM can be retrained to include the new behavior. Typical changes in mechanical parameters (such as shaft alignment or support structure stiffness) can be detected and quantified from vibration analysis. As the MBS model is fed back with the updated mechanical parameters and the RM model is retrained, this feedback loop can be regarded as an intermediate step to an application of physics-informed machine learning.

The method was evaluated using a MBS model of a 640 MW turbine generator. Two machine learning techniques were proposed for RM generation: an ANN and an SVR algorithm. It was found that RMSE significantly decreases for ANNs with 20 hidden-layer neurons or more and for 500 or more iterations of the training dataset. For SVR, the linear and RBF kernels yielded lower RMSE values, but the linear kernel was ultimately selected due to its comparative simplicity.

The two RM algorithms were shown to accurately predict single and two-plane unbalance simulated on a second multibody model with different bearing stiffness than those of the original model and with added signal noise. No significant advantages or disadvantages were found between the two machine learning methods, although it should be noted that the higher degree of complexity associated with ANNs and the difficulty to analyze its internal behavior compromises their reliability.

Overall, this method has the potential to become a new tool for continuous online monitoring and condition-based

maintenance of large scale steam turbines. Further experimental research must be done to assess the effect of faults that modify the stiffness of rotor elements, such as a lacing wire failure, shaft cracks, etc.

#### CONFLICT OF INTEREST STATEMENT

The authors declare no conflicts of interest.

#### REFERENCES

1. Statistical Review of World Energy, Statistical Review of World Energy 2020 – 69th Edition, London: BP p.l.c., 2020.
2. R. B. Randall, *Vibration-based Condition Monitoring: Industrial, Aerospace and Automotive Applications*, Chichester, West Sussex: John Wiley & Sons Ltd., 2011.
3. Z. Racic and J. Hidalgo, "Practical balancing of flexible rotors for power generation," in *Proc. ASME 2007 Int. Design Eng. Tech. Conf. Comput. Inf. Eng. Conf.*, Vol. 1, 21st Biennial Conference on Mechanical Vibration and Noise, Parts A, B, and C. Las Vegas, Nevada, USA. September 4–7, 2007. pp. 1143–1152. ASME. 2007.
4. M. Pingping, Z. Jingyu, Z. Hao, and H. Qingkai, "Multi-body dynamic simulation and vibration transmission characteristics of dual-rotor system for aeroengine with rubbing coupling faults," *J. Vibroeng.*, vol. 21, no. 7, pp. 1875–1887, 2019. DOI: [10.21595/jve.2019.20206](https://doi.org/10.21595/jve.2019.20206).
5. Y. Lei, B. Yang, X. Jiang, F. Jia, N. Li, and A. Nandi, "Applications of machine learning to machine fault diagnosis: A review and roadmap," *Mech. Syst. Signal Process.*, vol. 138, p. 106587, 2020. DOI: [10.1016/j.ymssp.2019.106587](https://doi.org/10.1016/j.ymssp.2019.106587).
6. H. Taplak, I. Uzmay, and Ö. Yıldırım, "Design of artificial neural network for rotor dynamics analysis of rotating machine systems," *J. Sci. Ind. Res.*, vol. 64, pp. 411–419, 2005.
7. R. Liu, B. Yang, E. Zio, and X. Chen, "Artificial intelligence for fault diagnosis of rotating machinery: A review," *Mech. Syst. Signal Process.*, vol. 108, pp. 33–47, 2018. DOI: [10.1016/j.ymssp.2018.02.016](https://doi.org/10.1016/j.ymssp.2018.02.016).
8. K. Vos, Z. Peng, C. Jenkins, M. R. Shahriar, P. Borghesani, and W. Wang, "Vibration-based anomaly detection using LSTM/SVM approaches," *Mech. Syst. Signal Process.*, vol. 169, p. 108752, 2022. DOI: [10.1016/j.ymssp.2021.108752](https://doi.org/10.1016/j.ymssp.2021.108752).
9. K. Yao, S. Fan, Y. Wang, J. Wan, D. Yang, and Y. Cao, "Anomaly detection of steam turbine with hierarchical pre-warning strategy," *IET Gener. Transm. Distrib.*, vol. 00, pp. 1–13, 2022. DOI: [10.1049/gtd2.12452](https://doi.org/10.1049/gtd2.12452).
10. X. Zhao, D. Ru, P. Wang, L. Gan, H. Wu, and Z. Zhong, "Fatigue life prediction of a supercritical steam turbine rotor based on neural networks," *Eng. Failure Anal.*, vol. 127, p. 105435, 2021. DOI: [10.1016/j.engfailanal.2021.105435](https://doi.org/10.1016/j.engfailanal.2021.105435).
11. W. M. Ashraf, Y. Rafique, G. M. Uddin, F. Riaz, M. Asim, M. Farooq, A. Hussain, C. A. Salmane, "Artificial intelligence based operational strategy development and implementation for vibration reduction of a supercritical steam turbine shaft bearing," *Alex. Eng. J.*, vol. 61, no. 3, pp. 1864–1880, 2022. DOI: [10.1016/j.aej.2021.07.039](https://doi.org/10.1016/j.aej.2021.07.039).
12. H. -S. Choi, J. An, S. Han, J. -G. Kim, J. -Y. Jung, J. Choi, G. Orzechowski, A. Mikkola and J. H. Choi, "Data-driven simulation for general-purpose multibody dynamics using

- Deep Neural networks,” *Multibody Syst. Dyn.*, vol. 51, no. 4, pp. 419–454, 2021. DOI: [10.1007/s11044-020-09772-8](https://doi.org/10.1007/s11044-020-09772-8).
13. G. E. Karniadakis, I. G. Kevrekidis, L. Lu, I. G. Kevrekidis, L. Lu, P. Perdikaris, S. Wang and L. Yang, “Physics-informed machine learning,” *Nat. Rev. Phys.*, vol. 3, pp. 422–440, 2021. DOI: [10.1038/s42254-021-00314-5](https://doi.org/10.1038/s42254-021-00314-5).
  14. E. J. Cross, S. J. Gibson, M. R. Jones, D. J. Pitchforth, S. Zhang, and T. J. Rogers, “Physics-informed machine learning for structural health monitoring,” in *Structural Health Monitoring Based on Data Science Techniques*. Structural Integrity, A. Cury, D. Ribeiro, F. Ubertini, M. D. Todd, Eds., vol. 21. Cham: Springer, 2022. DOI: [10.1007/978-3-030-81716-9\\_17](https://doi.org/10.1007/978-3-030-81716-9_17).
  15. Y. -P. Liu and Y. Altintas, “Predicting the position-dependent dynamics of machine tools using progressive network,” *Precis. Eng.*, vol. 73, pp. 409–422, 2022. DOI: [10.1016/j.precisioneng.2021.10.010](https://doi.org/10.1016/j.precisioneng.2021.10.010).
  16. A. Eddanguir and R. Benamar, “A discrete model for transverse vibration of a Cantilever Beam carrying multi lumped masses: Analogy with the continuous model,” in *Design and Modeling of Mechanical Systems*, Lecture Notes in Mechanical Engineering, M. Haddar, L. Romdhane, J. Louati, A. Ben Amara, Eds. Berlin, Heidelberg: Springer, 2013. DOI: [10.1007/978-3-642-37143-1\\_11](https://doi.org/10.1007/978-3-642-37143-1_11).
  17. A. A. Shabana, *Dynamics of Multibody Systems*, Second Edition, Cambridge University Press, Cambridge, UK, 1998.
  18. D. P. Kingma and J. L. Ba, “Adam: A method for stochastic optimization,” *International Conference on Learning Representations (ICLR)*, 2015 DOI: [10.48550/arXiv.1412.6980](https://doi.org/10.48550/arXiv.1412.6980).
  19. C. C. Aggarwal, *Neural Networks and Deep Learning: A Textbook*. New York: Springer, 2019.
  20. C. Cortes and V. N. Vapnik, “Support-vector networks,” *Mach. Learn.*, vol. 20, no. 3, pp. 273–297, 1995. DOI: [10.1007/BF00994018](https://doi.org/10.1007/BF00994018). S2CID 206787478.
  21. R. Nordmann, *Lateral Turbine and Generator Vibrations – Analysis and Mitigation*. Energiforsk, Stockholm, Sweden, 2016, ISBN: 978-91-7673-294-6.
  22. K. O. Achieng, “Modelling of soil moisture retention curve using machine learning techniques: Artificial and deep neural networks vs support vector regression models,” *Comput. Geosci.*, vol. 133, 2019. DOI: [10.1016/j.cageo.2019.104320](https://doi.org/10.1016/j.cageo.2019.104320).